4-7-2013

Mechanism of fatigue performance enhancement in a laser sintered superhard nanoparticles reinforced nanocomposite followed by laser shock peening

Dong Lin
Purdue University

Chang Ye
Purdue University

Yiliang Liao
Purdue University, liao10@purdue.edu

Sergey Suslov
Birck Nanotechnology Center, Purdue University, ssuslov@purdue.edu

Richard Liu
Purdue University

See next page for additional authors

Lin, Dong; Ye, Chang; Liao, Yiliang; Suslov, Sergey; Liu, Richard; and Cheng, Gary J., "Mechanism of fatigue performance enhancement in a laser sintered superhard nanoparticles reinforced nanocomposite followed by laser shock peening" (2013). *Birck and NCN Publications.* Paper 1385.
http://dx.doi.org/10.1063/1.4799154

AIP | Journal of Applied Physics

Mechanism of fatigue performance enhancement in a laser sintered superhard nanoparticles reinforced nanocomposite followed by laser shock peening

Dong Lin, Chang Ye, Yiliang Liao, Sergey Suslov, Richard Liu et al.

Citation: J. Appl. Phys. **113**, 133509 (2013); doi: 10.1063/1.4799154
View online: http://dx.doi.org/10.1063/1.4799154
View Table of Contents: http://jap.aip.org/resource/1/JAPIAU/v113/i13
Published by the AIP Publishing LLC.

Mechanism of fatigue performance enhancement in a laser sintered superhard nanoparticles reinforced nanocomposite followed by laser shock peening

Dong Lin,[1,2] Chang Ye,[1,2] Yiliang Liao,[1,2] Sergey Suslov,[2,3] Richard Liu,[1] and Gary J. Cheng[1,3,a)]
[1]*School of Industrial Engineering, Purdue University, West Lafayette, Indiana 47906, USA*
[2]*School of Materials Engineering, Purdue University, West Lafayette, Indiana 47906, USA*
[3]*Birck Nanotechnology Center, Purdue University, West Lafayette, Indiana 47906, USA*

(Received 16 December 2012; accepted 19 March 2013; published online 3 April 2013)

This study investigates the fundamental mechanism of fatigue performance enhancement during a novel hybrid manufacturing process, which combines laser sintering of superhard nanoparticles integrated nanocomposites and laser shock peening (LSP). Through laser sintering, TiN nanoparticles are integrated uniformly into iron matrix to form a nanocomposite layer near the surface of AISI4140 steel. LSP is then performed on the nanocomposite layer to generate interaction between nanoparticles and shock waves. The fundamental mechanism of fatigue performance enhancement is discussed in this paper. During laser shock interaction with the nanocomposites, the existence of nanoparticles increases the dislocation density and also helps to pin the dislocation movement. As a result, both dislocation density and residual stress are stabilized, which is beneficial for fatigue performance. © *2013 American Institute of Physics*. [http://dx.doi.org/10.1063/1.4799154]

I. INTRODUCTION

Laser shock peening (LSP) has been successfully applied to improve surface property of metallic components by generating a work hardened surface layer and introducing compressive residual stress.[1] LSP has been proved to be an effective way to improve surface hardness, wear resistance, corrosion resistance, and fatigue life.[2] However, the compressive residual stress generated by LSP is not stable at high working temperature.[3–5] Recently, warm laser shock peening (WLSP) was proposed to improve the residual stress stability of steel 4140 by dynamic strain aging (DSA) and dynamic precipitation (DP).[6] The diffusion of carbon and nitrogen atoms during DSA and generation of precipitation during DP help to pin the dislocation movement, therefore residual stress stability can be improved.[6] However, due to their small size, coherent boundaries and intrinsic mechanical properties, precipitates are not effective at resisting penetration of moving dislocations.[7] For example, it is easy for the mobile dislocations to penetrate Guinier-Preston zones in Al-Cu alloys.[8] In addition, WLSP is only effective at materials applicable to DSA and dynamic precipitation. As a result, many metals and alloys do not suit for WLSP.

Introducing harder particles into a metal matrix is an effective method to obstruct dislocation motion, thus, improving mechanical properties.[9] Metal matrix nanocomposites (MMNCs),[10,11] embedding nanoparticles into metal matrix, have been proposed to achieve this purpose. For instance, it has been reported the yield strength of as-cast aluminum alloy A356 increased by 50% with only 2 wt. % SiC nanoparticles dispersed as reinforcement material.[12] Nanoparticles have been also introduced into metal matrix by several other methods, such as vacuum sintering,[13] mechanochemical method,[14] laser cladding,[15] and ball milling.[16]

In this paper, a hybrid surface treatment combining laser sintering (LS) and laser shock peening is applied to introduce nanocomposite surface layer and improve mechanical properties. Laser sintering will be applied on AISI 4140 steel with a mixture of micro-sized iron powders and TiN nanoparticles. Laser shock peening will be used to enhance the mechanical properties of nanocomposite layer. During laser shock interaction with the nanocomposites, the existence of nanoparticles increases the dislocation density and also helps to pin the dislocation movement. As a result, both dislocation density and residual stress are stabilized, which is beneficial for fatigue performance. The composition of mixed structure, residual stress, and dislocation density will be studied by X-ray diffraction. The microstructures of samples after LS and LS plus LSP will be characterized by scanning electron microscope (SEM) and transmission electron microscope (TEM). The effect of these nanoparticles on the fatigue performance improvement by the hybrid manufacturing process will be investigated.

II. EXPERIMENTAL METHODS

Materials: The substrates were cut from low-alloyed steel AISI 4140 plate. The samples were first austenitized at 850 °C for 20 min followed by oil quench. After austenitization, the samples were tempered at 450 °C for 2 h and naturally cooled in vacuum furnace. The hardness of samples after heat treatment is 310 VHN (Vickers hardness number). The iron powders (average diameter of 4 μm) and TiN nanoparticles (average diameter of 20 nm) were selected for the coating materials.

a)Author to whom correspondence should be addressed. Electronic mail: gjcheng@purdue.edu.

LS experiments: Micro-sized iron powder and TiN nanoparticles were mixed together in solution by magnetic stirring. The solution was prepared by mixing 1.8 g iron powder and 0.2 g TiN nanoparticles into 4 wt. % polyvinyl alcohol (PVA) aqueous solution.[17] Mixed particles were coated on AISI 4140 surface by dip coating. Fig. 1(a) shows the cross-section after dip coating. Laser sintering was carried out by a Nd:YAG laser system under continuous-wave mode. The LS process was conducted in a protection chamber filled with N_2 gas in order to protect the sample from oxidation during LS. Fig. 1(b) represents cross-section after LS. The melting temperatures of TiN nanoparticle and iron powder are 2900 °C (Ref. 18) and 1600 °C, respectively. At selected laser intensity and scanning speed, the iron powders were melting while the TiN nanoparticles were kept solid during laser sintering process. The coated layer was melted together with substrate by laser sintering.

LSP experiments: LSP was performed after LS. Fig. 2 shows the diagram of laser shock peening. A Nd:YAG laser system (wavelength 1064 nm and pulse length 5 ns) was used as the energy source. The BK7 glass was used as confining medium because it has high shock impedance. Thin aluminum foil was chosen as the ablative coating to protect the sample surface. Laser intensity is the most important parameter of LSP. Fabbro model is used to estimate the laser intensity.[19] Laser shock peening conditions were: scanning speed 2 mm/s, frequency 8 HZ, beam size 1 mm, and overlap of beam 75%.

Microstructure characterization: A Bruker D8 Focus X-Ray diffractometer was used to detect the material composite with Cu-Kα source. Initial AISI 4140 sample, sample with LS, and sample with LS plus LSP were prepared for XRD measurement. A Hitachi S-4800 Field emission SEM was used to study the surface morphology and cross-sectional microstructures. A FEI Nova 200 focused ion beam (FIB) system was used to prepare TEM samples by lift-out method. The microstructure images were obtained by the FEI Titan system operating at 300 keV.

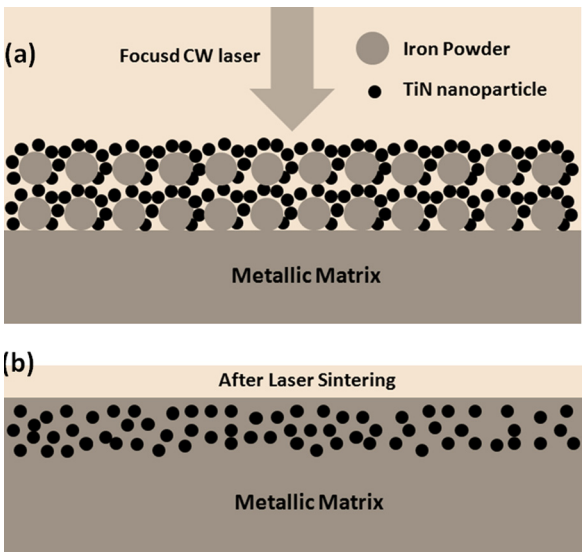

FIG. 1. Schematics of laser sintering of mixed iron and TiN particles pre-coated on AISI 4140 surface. Cross-section of sample (a) after surface coating and (b) after laser sintering.

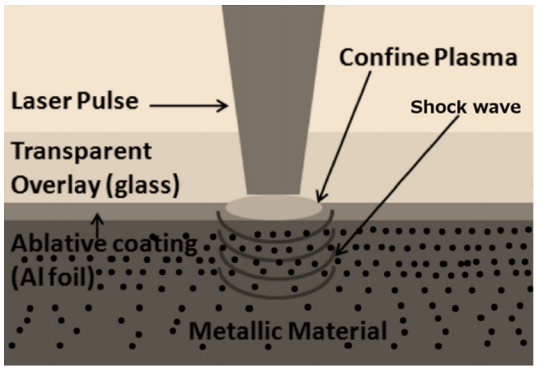

FIG. 2. Diagram of laser shock peening.

Mechanical property testing: The micro-hardness of initial AISI 4140, sample with LS, and sample with LS plus LSP was measured by Leco M-400-H micro-hardness instrument with 200 g load and 10 s holding time. The electrolytic polisher was used to etch steel samples by removing layer by layer in order to measure the in-depth micro-hardness.[6] The electrolytic polish solution was A1 solution from Proto Manufacturing, Inc. Three-point bending fatigue test was performed by the 100 KN MTS servo-hydraulic fatigue test machine. In the loading control mode, a sine wave function with frequency of 10 Hz was applied. The stress ration R was 0.1 for all fatigue tests, where R equals to $\sigma_{\min}/\sigma_{\max}$ ($\sigma_{\min}$ and $\sigma_{\max}$ are minimum stress and maximum stress, respectively). The maximal bending stress was $\sigma = 3PL/2bh^2$, where P is the applied load, L is the span for the bending fatigue test, b is the width of the specimen, and h is the thickness of the specimen. All the tests were carried out at room temperature and in a laboratory environment.

Residual stress measurements: The residual stress was measured by an X-ray micro-diffraction system (Bruker D8-Discover). The diameter of laser collimator was 0.1 mm. The peak was chosen to do the stress analysis, which is related to the 2θ angle of 123.916°.[6] The XRD source is $CoK_{\alpha 1}$ using $\sin^2\psi$ method as analyzed method.[20] The interference lines of the steel phase were measured at 11ψ angles from $-50°$ to $+50°$.[20] The full width at half maximum (FWHM) integral value was used to evaluate the X-ray peak broadenings by removing the $K_{\alpha 2}$ signals.[6] Relative dislocation density was measured by the FWHM value at the 90° X-ray incidence angle of the Bragg diffraction peaks.[20]

III. RESULTS AND DISCUSSION

A. Scheme of the hybrid manufacturing process

1. Selection of laser sintering processing conditions

Laser intensity and scanning speed are two of the most important parameters for the LS process. This is because both surface finish and cross-section of laser sintered layer are affected by these two parameters.[21–23] The ND:YAG laser system was working at the CW mode and its energy during LS was 94 W. Spot size of laser beam and scanning speed was 0.8 mm and 2 mm/s, respectively. Laser sintering

was performed in a protection chamber filled with N_2 gas in order to protect the samples from oxidation. A layer of mixture of iron powders and TiN nanoparticles was coated prior to LS. The volume ratio of TiN nanoparticles is approximately 9%. The reason for choosing this volume ratio was for better strengthening of matrix with Orowan strengthen, dislocation density strengthen, etc. The step after LS of hybrid process is LSP. The effect of LSP on the matrix strengthening is enhanced by this volume fraction, which is discussed in Sec. III D in detail.

2. Selection of laser shock peening processing conditions

One of the most important parameters during LSP is laser intensity, which decides the shock pressure.[24] In this study, BK-7 glass was chosen as confining medium, which has a shock impedance of 1.44e6 g cm^{-2} s^{-1}.[24] The laser induced-peak pressure can be estimated by Fabbro model: $P(I_0) = 0.01\sqrt{\alpha/2\alpha+3}\sqrt{Z(\mathrm{g/cm^2s})}\sqrt{I_0(\mathrm{GW/cm^2})}$,[25] where α and I_0 are portion of absorbed energy contributed to thermal energy of plasma and laser intensity, respectively. The value of Z ($Z = 2Z_1Z_2/(Z_1+Z_2)$) is the reduced shock impedance between target material (AISI 4140 steel: shock impedance 3.96e6 g cm^{-2} s^{-1}) and confining medium. It can be also estimated by $Z = \rho D$, where ρ is material density and D is shock velocity.[26]

Liao *et al.*[27] found that surface hardness of steel 4140 was saturated at the laser intensity over 4 GW cm^{-2} because the plastic deformation limit was reached when the shock pressure was larger than twice of Hugoniot elastic limit (HEL) of as-received materials.[27,28] Surface hardness under various laser intensities (from 1 GW cm^{-2} to 4 GW cm^{-2}) was measured in Fig. 3 in order to investigate surface hardening effect of shock pressure. Surface micro-hardness is related to dislocation density: $H = H^* + \alpha G b\sqrt{\rho}$, where H^*, α, G are material's constants, b is Burger's vector, and ρ is the dislocation density.[29] The LSP was performed to both as-received samples and laser sintered samples. The estimated peak plasma pressure increases with increasing laser intensities based on Fabbro's model.[24] Surface hardness is increased with enhanced laser intensities for both kinds of samples. For example, the Vickers's hardness of as received samples is increased from 310 VHN to 361 VHN after LSP (1 GW cm^{-2}). The surface hardness of as received material at the laser intensity of 4 GW cm^{-2} is 387 VH, which is around 25% improvement from the base material. After integrating 9% volume percentage of TiN nanoparticles into iron matrix, the surface hardness increases to 410 VHN. LSP was performed after LS for further surface hardening effect. The surface hardness after hybrid manufacturing process increases as the laser intensity increasing. It reaches a peak hardness value of 499 VH at the laser intensity of 4 GW cm^{-2}, which is around 61% increase from base material. Therefore, hybrid manufacturing process has a higher surface hardening effect than only laser integrated nanocomposites or LSP.

The in-depth micro-hardness after hybrid manufacturing process is shown in Fig. 4. The laser intensity was 3 GW cm^{-2} during LSP. The thickness of Fe/TiN nanocomposites layer is around 70 μm. The micro-hardness gradually reduces from the top surface of laser sintered layer to the base material. The hardness at the depth of 200 μm is around 380 VH, which is equivalent to the surface hardness after the LSP in Fig. 3.

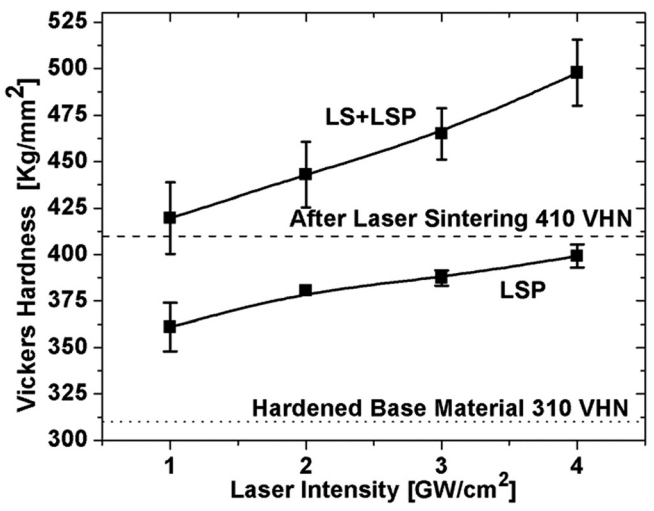

FIG. 3. Surface micro-hardness of various samples: non-treated sample, base material with LSP, base material with LS and LS plus LSP.

B. Hybrid microstructures induced by hybrid manufacturing process

1. TiN nanoparticle integrated nanocomposite by laser sintering

The surface morphology and cross-sectional microstructure after laser sintering are important for the mechanical properties of Fe/TiN nanocomposites. Figs. 5(a) and 5(b) show surface morphology after LS. The inset image in Fig. 5(a) represents higher magnification of surface morphology. Fig. 5(b) was obtained from (a) by tilting 52°. It shows that a layer of nanoparticles was sintered on the top surface, which may be caused by the drifting of nanoparticles during coating process. The cross-section of laser sintered layer is shown in

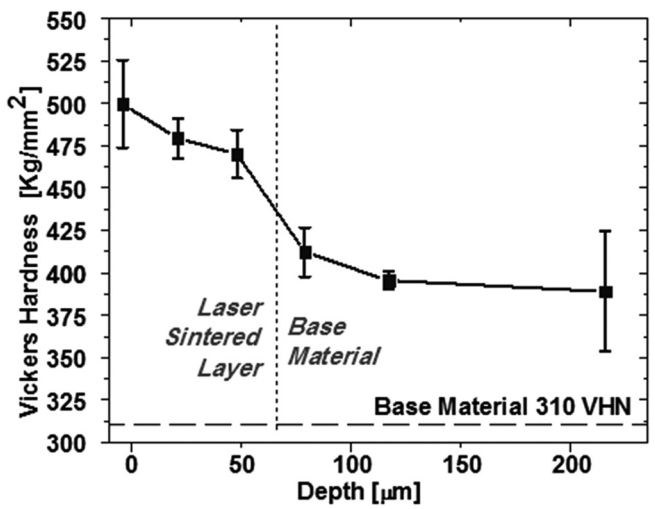

FIG. 4. In depth micro-hardness after hybrid manufacturing process.

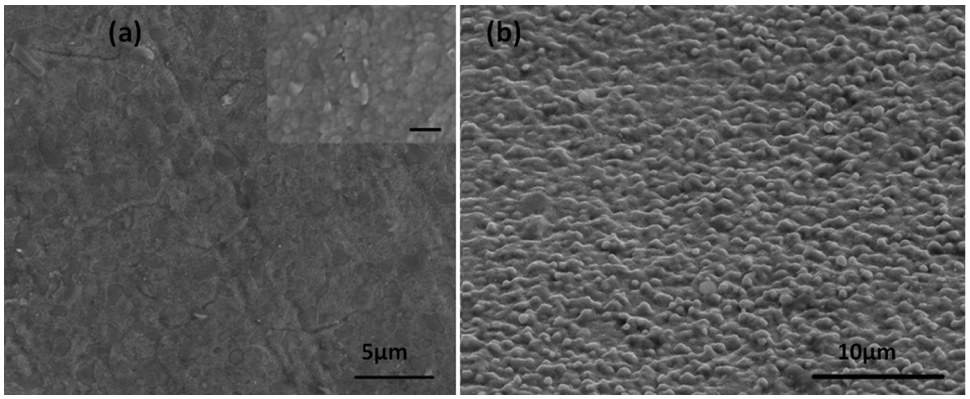

FIG. 5. (a) Surface morphology after laser sintering, (scale bar of inset image: 250 nm), (b) view of (a) while tilting at 52°.

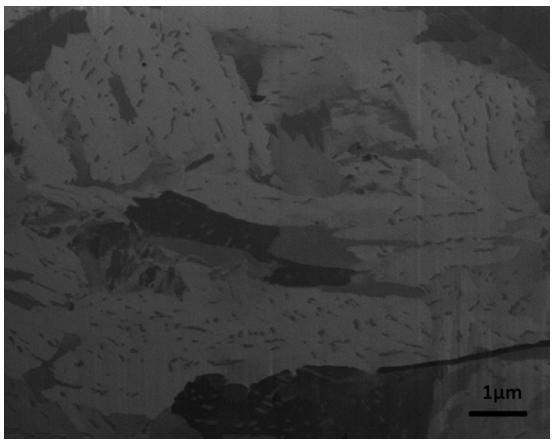

FIG. 6. SEM image of cross-sectional Fe/TiN nanocomposites after laser sintering.

Fig. 6. The size of iron grains is from several hundred nanometers to several micrometers. The TiN nanoparticles (marked in Fig. 6) are evenly dispersed in the cross-section of Fe/TiN nanocomposites. It demonstrates the feasibility of dispersing large scale of nanoparticles into matrix by laser sintering. The melting temperature of microsized iron powder (average size 4 μm) and TiN nanoparticle (average size 20 nm) is 1600 °C and 2900 °C, respectively.[18] Under selected laser intensity, iron powders were melted during LS process while TiN nanoparticles were keeping solid.

The microstructure of TEM images after LS is shown in Fig. 7. Fig. 7(a) is the bright field TEM image, while Fig. 7(b) is the dark field image of Fig. 7(a). The insetted diffraction pattern in Fig. 7(a) is a selected area electron diffraction on the spots of nanoparticles. Bright spots in Fig. 7(b) are TiN nanoparticles. PVA was used to separate nanoparticles during dip coating and was burned during LS. The cross-sectional TEM and SEM pictures demonstrate that nanoparticles did not aggregate during melting iron powders. Fig. 8 shows cross-sectional microstructure of as-received steel AISI 4140 sample. The initial microstructure of quenched and tempered steel contains low density of lath-type precipitates (Fe_3C type).[6]

The compositions of samples after coating and after LS were examined by X-ray diffraction, which is represented in Fig. 9. LS process was conducted in the N_2 gas in order to protect iron powder and TiN nanoparticles from oxidization. The comparison between the XRD curves after coating and the one after LS shows that all TiN peaks survived to laser sintering.

2. Microstructures after hybrid manufacturing process

The mechanical behaviors of metallic materials may be greatly affected by microstructures. It is of interest to study the microstructure after LSP, which is the second step of the hybrid manufacturing process. Ye *et al.* investigated the cross-sectional microstructure after LSP.[6] Pile-up of

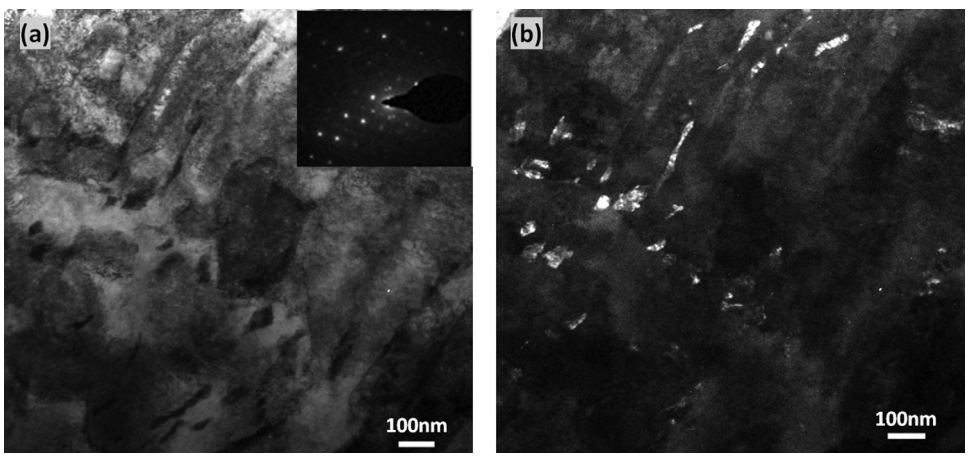

FIG. 7. TEM images of cross-section of laser sintered layer after LS. (a) Bright field image and (b) dark field image with selected area electron diffraction on the spots of nanoparticles.

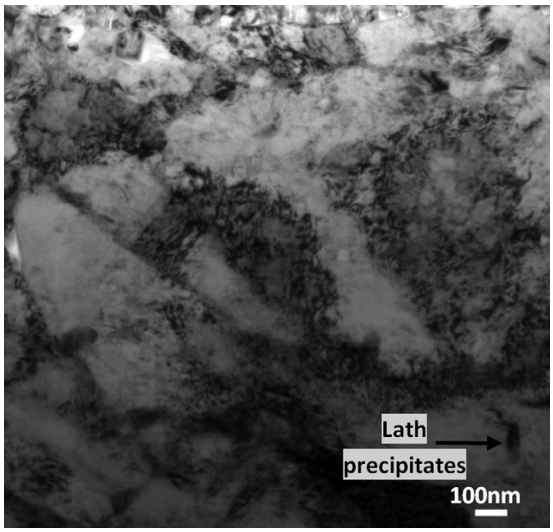

FIG. 8. TEM images of as-received AISI4140 steel sample after heat treatment.

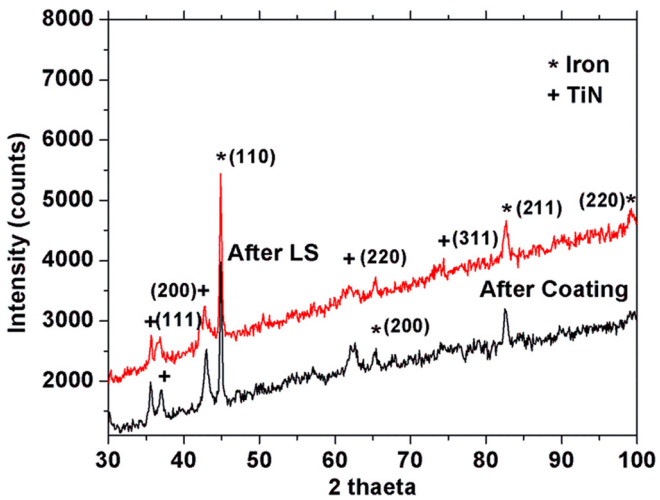

FIG. 9. Surface X-ray diffraction pattern after coating, and after LS.

localized dislocations and lamellar dislocation boundaries was observed at different positions.[6,30] The shear bands were generated by high strain rate deformation.[31] Figs. 10(a) and 10(b) show large area dislocation distribution in the laser sintered Fe/TiN nanocomposite layer after hybrid manufacturing process. The left side of dot line in Fig. 10(a) is the top surface of Fe/TiN nanocomposites. The original diameters of marked TiN nanoparticles in Fig. 10(b) are from 20 to 75 nm.[18] The laminar shape of nanoparticles, which were marked in Fig. 10(b), was formed by several nanoparticles.

C. Strengthening mechanisms of superhard TiN nanoparticles integrated nanocomposites

The strengthening mechanism of MMNCs has been studied recently,[32–34] and four strengthening mechanisms were proposed to explain the strengthening enhancement. These mechanisms include dislocation density enhancement by thermal mismatch and LSP, Orowan strengthening, Hall-Petch strengthening, and load transfer.[33] The improvements of yield strength of TiN nanoparticle integrated nanocomposites can be expressed as[34]

$$\sigma_{yc} = \sigma_{ym}(1+f_{Load})(1+f_d)(1+f_{Orowan})(1+f_{Hall-petch}), \quad (1)$$

where σ_{yc} is the yield strength of Fe/TiN nanocomposites, σ_{ym} is the yield strength of iron matrix, f_{Load}, f_d, f_{Orowan}, $f_{Hall-petch}$ are the enhancement factors associated with loading bear, dislocation density strengthening, Orowan strengthening, and Hall-Petch strengthening, respectively.

1. Effect of nanoparticles on dislocation density after laser shock peening

After the hybrid manufacturing process, dislocations density can be enhanced through relaxation of thermal residual stress during laser sintering and laser shock peening.[35] Based on the calculation of De Cicco *et al.*,[33] the dislocation density due to the existence of nanoparticles plays a very important role in strengthening enhancement for MMNCs.

Dislocation density increase by thermal residual stress will be discussed first. Ashby and Johnson *et al.*[36] found that the creation of thermally stimulated dislocation is energetically favorable. They also noticed that the dislocation density increases with increasing the volume fraction of nanoparticles and decreasing the size of nanoparticles.[11] The simplest mechanism to relief stress for short fibers and

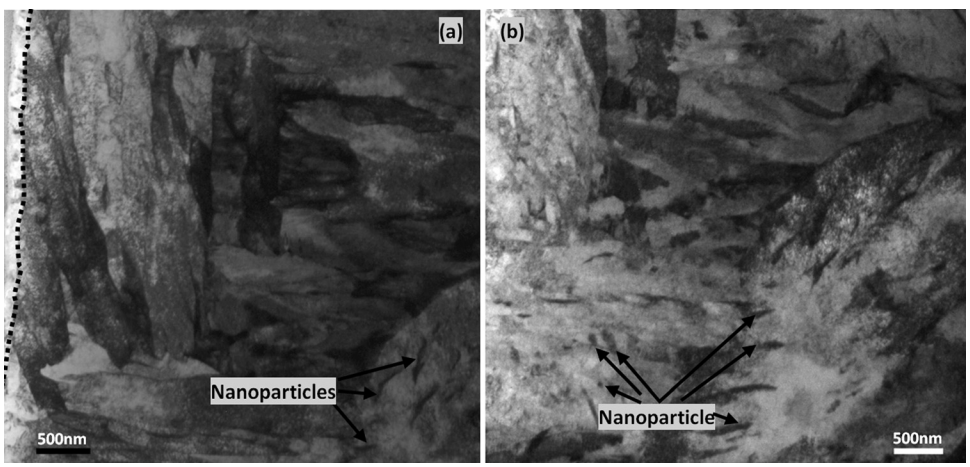

FIG. 10. Dislocation distribution in the Fe/TiN nanocomposites after hybrid manufacturing process, dislocation and nanoparticle distribution (a) near the top surface and (b) in the cross section.

particles enhanced matrix is to punch out a dislocation loop into the matrix.[35] Arsenault *et al.* assumed that the misfit strain is relaxed by punching dislocation loops so that they can estimate strengthening effect.[11,35,37] The dislocation density increase by thermal mismatch can be written by[37]

$$\Delta\rho = \frac{\Delta\alpha\Delta TNA}{b}, \tag{2}$$

where $\Delta\alpha\Delta T$ is thermal misfit strain, N is the number of particles, b is the Burgers vector, and A is the total surface of each particle. Based on Eq. (2), lower dislocation density increase would be expected when the nanoparticles become more spherical.[35,37]

LSP was performed after LS. The dislocation density was increased significantly by the existence of nanoparticles after laser shock peening due to dislocation pinning of the nanoparticles.[27] The Orowan's equation describes the metal plastic deformation thanks to the mechanisms of generation and motion of dislocations[28,38–40]

$$\rho = \varepsilon^p / K\chi b, \tag{3-1}$$

$$\dot{\varepsilon} = \rho v b, \tag{3-2}$$

where K is a factor concerned of dislocation, approximately equals to 1.25,[34] and $\chi \approx \frac{1}{\sqrt{\rho}}$ is the average distance of dislocation, v is the velocity.

The plastic deformation can be calculated by considering the HEL[28]

$$\varepsilon^p = \frac{2HEL}{3\lambda + 2\mu}\left(\frac{P}{HEL} - 1\right), \tag{4}$$

where λ and μ are Lame elastic constants (GPa), and P the shock pressure. The plastic deformation starts at HEL, saturates at 2HEL, and has a linear relation with P.[28] The optical pressure driving ε^p to saturation is between 2 and 2.5 *HEL* and the laser shock pressure in this report was around 2 *HEL*.[28]

The improvement factor related to dislocation density is as follows:[34]

$$f_d = kG_m b\sqrt{\rho}/\sigma_{ym}, \tag{5}$$

where k is a constant, approximately equal to 1.25, ρ is the enhanced dislocation density contributed by two steps of this hybrid manufacturing process: residual plastic strain caused by difference in thermal expansion coefficient during post-laser sintering cooling and also laser shock peening. The enhanced dislocation density can be calculated by combining Eqs. (3) and (4).

The near-surface work hardening, which is related to dislocation density, can be measured indirectly by FWHM values.[4,41] Fig. 11 exhibits the FWHM values of base material, samples after LSP, samples after LS, and samples after LS plus LSP. The FWHM value after LS (1.00) is higher than base material (0.70) and LSP (0.83), which is contributed by the thermal stress relaxation during cooling. FWHM reaches the highest value of 1.10 after LS plus LSP, which indicates that it has the highest defect density. The nanoparticles help to further increase dislocation density during LSP for the second step of hybrid manufacturing.[27] These measured FWHM values are in agreement with the surface microhardness in Fig. 3 because the surface hardening has a linear relationship to $\sqrt{\rho}$. The surface hardness after LS is higher than after LSP, and LS plus LSP further improves surface hardening effect by increasing dislocation density. With higher dislocation density, the hybrid manufacturing process produces higher resistance for crack initiation.[42]

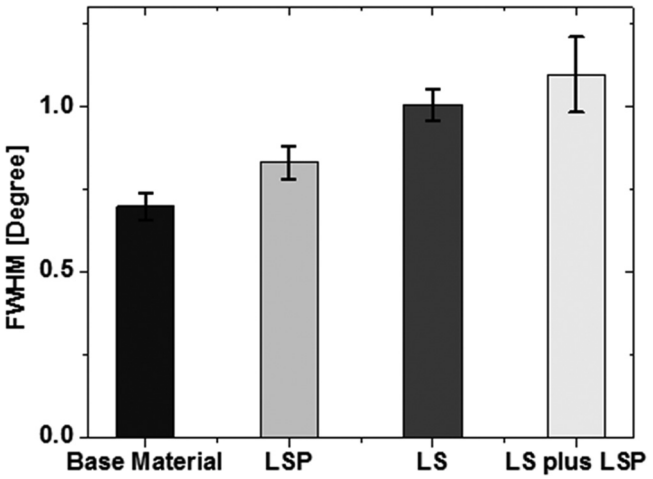

FIG. 11. FWHM values of base material, sample after LSP, sample after LS, and sample after LS plus LSP.

2. Dislocation pinning effects

Dislocation pinning by closely spaced hard particles is named as Orowan strengthening.[34] Orowan strengthening is often used to explain strengthening in composites containing fine particles.[43,44] The strengthening effect is significant in MMNCs due to the presence of uniformly dispersed nanoparticles (smaller than ~100 nm).[34] Even for a small volume fraction of nanoparticles (<1%), Orowan bowing is necessary for dislocations to bypass nanoparticles.[34,35] Shao *et al.* used Orowan dislocation bowing mechanism to explain the improvement of hardness in nanocomposite Ni/Al_2O_3 films.[34,43] Orowan strengthening loop was observed by Thilly *et al.* and the deformation mechanism was used to simulate the mechanical performance of Cu/Nb nanocomposites.[34,44] The thermal mismatch during laser sintering and subsequent laser shock peening generated enough plastic deformation in iron matrix and dislocation loops around vicinity of TiN nanoparticles and the nanoparticles are expected to exert back stress on dislocation movement.[34,45] Orowan strengthening effect can be given by[46]

$$\Delta\sigma_{Orowan} = M\frac{0.4Gb}{\pi(1-\nu)^{1/2}}\frac{\ln(\sqrt{2/3}d/b)}{\sqrt{2/3}d(\sqrt{\pi/(4V_P-1)})}, \tag{6}$$

$$G = \frac{E}{2(1+\nu)}, \tag{7}$$

$$f_{Orowan} = \Delta\sigma_{Orowan}/\sigma_{ym}, \tag{8}$$

where M is the mean orientation factor, G is the shear modulus of the matrix (Pa), b is the Burger's vector, ν is Poisson's

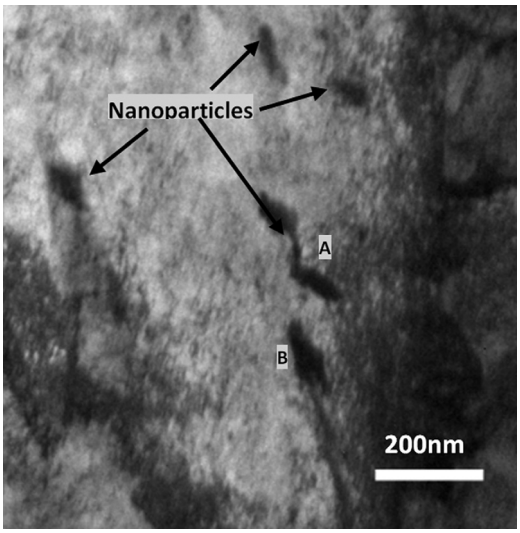

FIG. 12. Interaction between TiN nanoparticles and dislocations in iron grain.

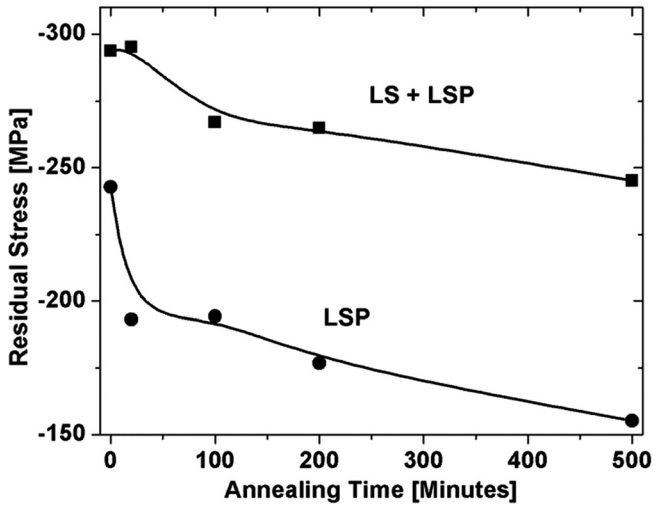

FIG. 13. Thermal stability of residual stress annealing at 350 °C at different times for LSP and LS plus LSP samples.

ratio, E is elastic modulus of iron, V_P is volume fraction of nanoparticles, and d is the nanoparticle diameter.

Closely spaced superhard TiN nanoparticles in a grain after LS plus LSP are shown in Fig. 13. In order to overcome the local obstacles at room temperature, dislocations have to cut through or bypass the nanoparticles.[27] In MMNCs, the dislocation–nanoparticle interaction mechanism is mainly considered to be Orowan looping.[32,34,47] Superhard TiN nanoparticles contribute to the Orowan strengthening by increasing critical shear stress τ_p, which is the minimal external stress for overcoming dislocation-nanoparticle interaction forces.[27,48] Nembash *et al.* proposed τ_p function by taking into account of actual distribution of particles size[27,48]

$$\tau_p(d, V_p) = \frac{0.9bG}{\pi w_L d\sqrt{1-\upsilon}} \ln\left(\frac{w_D d}{b}\right)\left[\frac{\ln(w_D d/b)}{\ln(w_L d/2b)}\right]^{1/2}, \quad (9)$$

$$w_L = \sqrt{\pi w_q / f} - 2w_r, \quad (10)$$

$$w_D^{-1} = w_L^{-1} + (2w_r)^{-1}, \quad (11)$$

where w_r and w_q are the mean radius and mean area of nanoparticles intersection with glide plane. Equation (9) indicates that resolved shear stress is related to nanoparticle size (d) and volume fraction V_p. Nanoparticles induced stress field is enhanced thus larger Orowan loops are formed in order to bypass for larger nanoparticles, while dislocations have to bend more due to decreased free space by increased volume fraction.[27] It means dislocation pinning effect can be enhanced with larger nanoparticles and higher volume fraction of nanoparticles. Fig. 12 shows the interaction between TiN nanoparticles and dislocations in a grain. The dislocation density at the right side of nanoparticles A and B is higher than the left side, which means nanoparticles resist dislocation movement.

The stability of compressive residual stress is considered as important as the magnitude of residual stress because it retards fatigue crack initiation.[6,24] It was discovered by Harada and Mori[49] that plastic deformation tends to be increased by reducing flow stress under higher processing temperature. Therefore, it is important to keep the compressive residual stress stable under annealing temperature. The relaxation of compressive residual stress can be caused by dislocation movement. Different mechanisms of resisting dislocation movement were proposed, such as dislocation blocking by solute atoms, precipitate particles, and dislocation pinning at different slip planes.[7] The stability of residual stress under different annealing temperature is still a challenge for LSP,[24] so that WLSP was proposed to improve dislocation stability by generating solute atoms and precipitate particles to pin dislocation movement.[6] However, WLSP can only be applied to certain materials, such as steels with high carbon content; therefore, superhard TiN nanoparticles integrated nanocomposites were designed for broad application. The compressive residual stress stabilities of as received sample after LSP and LS plus LSP under the annealing temperature of 350 °C in the furnace were monitored in Fig. 13. These two curves indicate that samples after hybrid manufacturing process have better residual stress stability, especially at the beginning of 20 min. The residual stress remained stable after 20 min of annealing. It only decreases for 16.6% after 500 min of annealing. The residual stress of LSP processed base material lost around 20% after 20 min of annealing. It had a total of 36% decrease of compressive residual stress after annealing 500 min. Hybrid manufacturing process also generated higher initial residual stress compared to LSP. With better residual stress stability, samples after hybrid manufacturing process are expected to have higher resistance for crack initiation.

Near surface work hardening is also beneficial for crack initiation by limiting plastic deformation.[24] Many components and structures are working at the elevated temperature, which means the thermal stability is important for real working conditions. Artificial annealing tests of LSP and LS plus LSP samples were carried out at 350 °C in the furnace. Fig. 14 shows the hardness variation at different annealing times. It takes 20 min for hybrid manufactured samples to reach the peak hardness (466.6 VHN), which is almost the same as the initial hardness (465 VHN). The highest hardness is reached

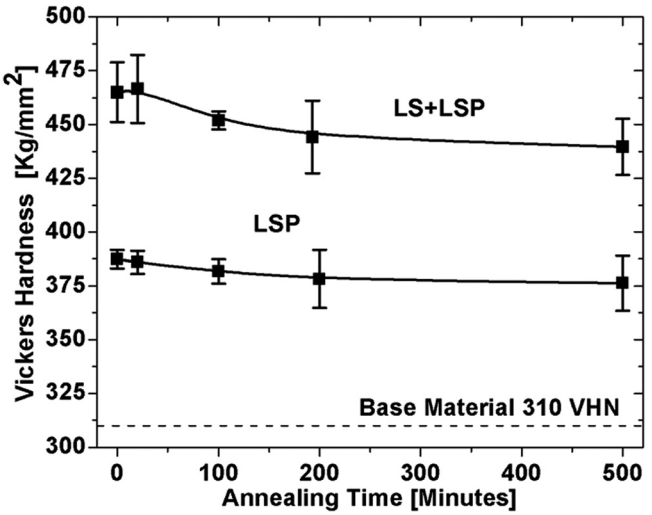

FIG. 14. Surface hardness stability at annealing temperature of 350 °C for LSP and LS plus LSP samples.

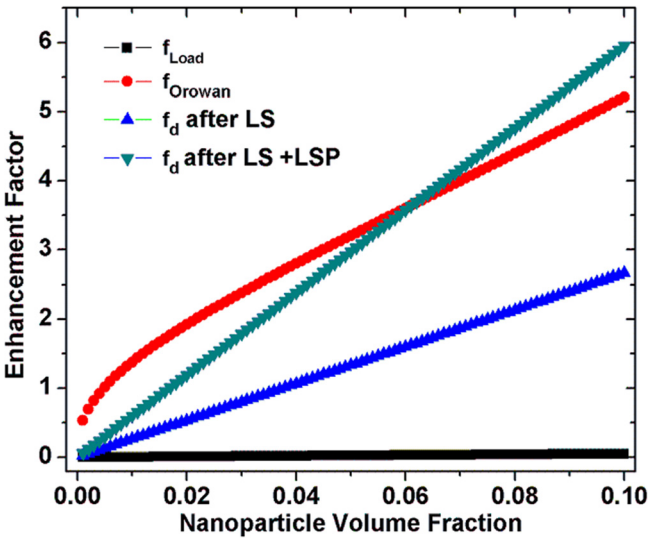

FIG. 15. Three enhancement factors of f_{Load}, f_{Orowan}, and f_d as function of the volume fraction of TiN nanoparticles in iron matrix after LS and after LS plus LSP.

when the dispersed TiN nanoparticles obtain a fine dispersion of coherent with surrounded matrix by elastic strain.[6] As the annealing time increases, the relaxation of the dislocations is pinned by the TiN nanoparticles, which provide localized stress field that hinders the dislocation climbing or gliding.[6] After hybrid manufacturing process, high density of dislocations were generated due to the shock wave interaction with the TiN nanoparticles and thermal mismatch with matrix.[34] These nanoparticles increase the glide resistance when dislocation moves, interact and change their distribution and density.[6] Surface hardness of both kinds of samples remained stable after 500 annealing, which tends to protect samples for crack initiation even under elevated working temperature.

3. Other strengthening mechanisms

Due to the laser integrated method, the TiN nanoparticles are strongly bonded together with matrix at atomic level.[50] For particulate-reinforced composite, f_{Load} can be generally written as[34]

$$f_{Load} = 0.5V_P. \tag{12}$$

Another strengthening mechanism is Hall-Petch strengthening by refining the grain size.[32] The $f_{Hall-petch}$ can be summarized as follows:[32]

$$f_{Hall-Petch} = k_y d_m^{-1/2}/\sigma_{ym}, \tag{13}$$

where k_y is constant and d_m is the grain size of matrix. Goh *et al.*[32] found grain size change was negligible when adding 2 vol. % of Y_2O_3 nanoparticles in Mg matrix. The decrease in grain size is not significant by adding low volume fraction of nanoparticles, so that Hall-Petch effect is not counted in this paper.

4. Strengthening enhancement factors

Yield strength enhancement factors, after hybrid manufacturing process, of various strengthening mechanisms as function of the volume fraction of TiN nanoparticles are represented in Fig. 15. Based on Eqs. (6) and (12), load transfer strengthening and Orowan strengthening are not affected by the dislocation density change, which means these two enhancement factors would not change after LSP. The enhancement factors of f_{Load}, f_{Orowan}, and f_d increase monotonically with increasing volume fraction (volume fraction lower than 0.1) of TiN nanoparticles in iron matrix. The enhancement factor of f_{Load} is small when the volume fraction is low. While in Fe/TiN nanocomposites, the enhancement factor of f_{Orowan} is larger than f_d after laser sintering. However, dislocation density can be further increased by LSP so that dislocation enhancement factor is also further improved. For the volume fraction (0.09) of TiN nanoparticle in this paper, dislocation density strengthening plays the more important role than Orowan and load transfer enhancement mechanisms after hybrid manufacturing process.

D. Fatigue performance

The stress-lifespan (S-N) tests were conducted for three process conditions: (1) solution treatment; (2) laser shock peening; and (3) laser sintering plus laser shock peening, which are shown in Fig. 16. The effect of LSP and LS plus LSP on fatigue performance can be compared by both fatigue strength and fatigue limit.[24,51] It is clearly shown that hybrid manufacturing process, compared to LSP, has a better fatigue performance. For example, for a fatigue life of a million cycles, the fatigue strength for non-treated, LSP and LS plus LSP is approximately 600, 700, and 800 MPa, respectively. In addition, for applied stress of 1200 MPa, the fatigue lives of LS plus LSP and LSP are 5.6 and 3.9 times of non-treated samples. Along with other popular surface treatment techniques, like LSP, shot peening (SP), and deep rolling (DR), the hybrid manufacturing process also represents higher improvement of fatigue life for high cycle regime (HCR) than low cycle regime (LCR).[6]

LSP improved fatigue performance by surface hardening and introduction of residual stress,[6,24,51] while MMNCs strengthen metal matrix by mainly introducing Orowan strengthening and dislocation strengthening.[34] The hybrid

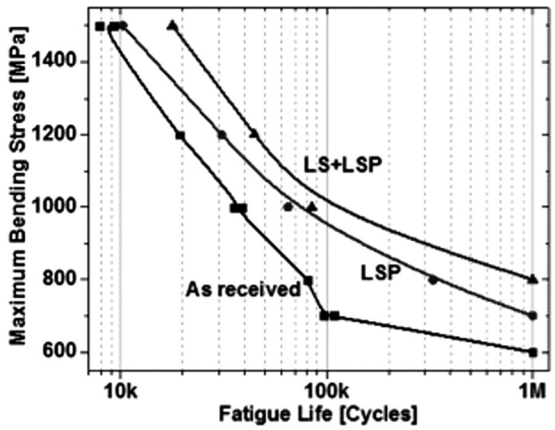

FIG. 16. Fatigue test of as-received AISI 4140 sample (non-treated), sample after LSP and sample after LS plus LSP.

manufacturing technique combines both benefits of LSP and MMNCs for fatigue life improvement. It provides a greater hardness enhancement, higher dislocation density, better dislocation pinning, and also higher thermal stable residual stress. Higher hardness links to higher dislocation density, which is from thermal mismatch of cooling after laser sintering and following laser shock peening process. Improvement of dislocations density after hybrid manufacturing process results in a higher dislocation density strengthening. While the dislocation density enhancement factor for hybrid process is approximately 5.4, which is much higher than the enhancement factor of LS of 2.4. While the Oworan strengthening of superhard TiN nanoparticles in Fe/Ti nanocomposites induces better dislocation pinning, thus providing better thermal stability of residual stress. The calculated Orowan strengthening factor is around 4.8. The higher magnitude and better thermal stability of residual stress are demonstrated in Fig. 13. Compared to former surface processing techniques, including SP, DR, and LSP, hybrid manufacturing process has greater potential for the enhancement of mechanical properties from above beneficial. Therefore, this hybrid manufacturing technique is expected to have brighter application future for industry.

IV. CONCLUSION

In this paper, the fatigue performance of LS plus LSP was investigated. The TiN nanoparticles were integrated into iron matrix by laser sintering. The TiN nanoparticles help to further increase the dislocation density by laser shock peening and also pin the dislocation movement thus increasing the residual stress stability. Compared to laser shock peening, the surface hardness and defect density are increased by LS plus LSP. After the hybrid manufacturing process, the fatigue life was improved by better compressive residual stress stability, strength stability, and higher work hardening effect. Both compressive residual stress (which retards crack propagation) and work hardening (which retards crack initiation) are beneficial to the fatigue life of the components.

[1]C. S. Montross, T. Wei, L. Ye, G. Clark, and Y.-W. Mai, "Laser shock processing and its effects on microstructure and properties of metal alloys: A review," Int. J. Fatigue **24**(10), 1021–1036 (2002).
[2]P. Peyre and R. Fabbro, "Laser shock processing: A review of the physics and applications," Opt. Quantum Electron. **27**(12), 1213–1229 (1995).
[3]I. Nikitin and I. Altenberger, "Comparison of the fatigue behavior and residual stress stability of laser-shock peened and deep rolled austenitic stainless steel AISI 304 in the temperature range 25–600 °C," Mater. Sci. Eng., A **465**(1–2), 176–182 (2007).
[4]I. Nikitin, B. Scholtes, H. J. Maier, and I. Altenberger, "High temperature fatigue behavior and residual stress stability of laser-shock peened and deep rolled austenitic steel AISI 304," Scr. Mater. **50**(10), 1345–1350 (2004).
[5]P. Juijerm and I. Altenberger, "Residual stress relaxation of deep-rolled Al-Mg-Si-Cu alloy during cyclic loading at elevated temperatures," Scr. Mater. **55**(12), 1111 (2006).
[6]C. Ye, S. Suslov, B. J. Kim, E. A. Stach, and G. J. Cheng, "Fatigue performance improvement in AISI 4140 steel by dynamic strain aging and dynamic precipitation during warm laser shock peening," Acta Mater. **59**(3), 1014–1025 (2011).
[7]K. Lu, L. Lu, and S. Suresh, "Strengthening materials by engineering coherent internal boundaries at the nanoscale," Science **324**(5925), 349–352 (2009).
[8]A. B. Witney, P. G. Sanders, J. R. Weertman, and J. A. Eastman, "Fatigue of nanocrystalline copper," Scr. Metall. Mater. **33**, 2025 (1995).
[9]G. Cao, H. Konishi, and X. Li, "Mechanical properties and microstructure of Mg/SiC nanocomposites fabricated by ultrasonic cavitation based nanomanufacturing, J. Manuf. Sci. Eng. **130**(3), 031105 (2008).
[10]Y. Yang and X. Li, "Ultrasonic cavitation based nanomanufacturing of bulk aluminum matrix nanocomposites," J. Manuf. Sci. Eng. **129**(3), 497–501 (2007).
[11]R. J. Arsenault, L. Wang, and C. R. Feng, "Strengthening of composites due to microstructural changes in the matrix," Acta Metall. Mater. **39**(1), 47–57 (1991).
[12]Y. Yang, J. Lan, and X. Li, "Study on bulk aluminum matrix nanocomposite fabricated by ultrasonic dispersion of nano-sized SiC particles in molten aluminum alloy," Mater. Sci. Eng., A **380**(1–2), 378–383 (2004).
[13]Y. C. Luo and D. Y. Li, "New wear-resistant material: Nano-TiN/TiC/TiNi composite," J. Mater. Sci.**36**(19), 4695–4702 (2001).
[14]F. Shehata, A. Fathy, M. Abdelhameed, and S. F. Moustafa, "Preparation and properties of Al2O3 nanoparticle reinforced copper matrix composites by in situ processing," Mater. Des. **30**(7), 2756–2762 (2009).
[15]S. Yu, Y. Liu, L. Ren, and W. Li, "Development of laser-cladding layers containing nano-Al_2O_3 nanoparticles for wear-resistance materials," Metall. Mater. Trans. A **37**(12), 3639–3645 (2006).
[16]E. Yarrapareddy and R. Kovacevic, "Synthesis and characterization of laser-based direct metal deposited nano-particles reinforced surface coatings for industrial slurry erosion applications," Surf. Coat. Technol. **202**(10), 1951–1965 (2008).
[17]W. T. Tsai, T. H. Lai, and J. T. Lee, "Laser surface alloying of stainless steel with silicon nitride," Mater. Sci. Eng., A **183**(1–2), 239–245 (1994).
[18]D. Lin, S. Suslov, C. Ye, Y. Liao, C. R. Liu, and G. J. Cheng, "Laser assisted embedding of nanoparticles into metallic materials," Appl. Surf. Sci. **258**(7), 2289–2296 (2012).
[19]P. Ballard, J. Fournier, R. Fabrro, and J. Frelat, "Residual stresses induced by laser shocks," J. Phys. IV **01**(C3), 487–494 (1991).
[20]H. P. Klug and L. E. Alexander J. Appl. Crystallogr. **8**(573), 4 (1975).
[21]S. Das, "Physical aspects of process control in selective laser sintering of metals," Adv. Eng. Mater. **5**(10), 701–711 (2003).
[22]J. P. Kruth, P. Mercelis, J. Van Vaerenbergh, L. Froyen, and M. Rombouts, "Binding mechanisms in selective laser sintering and selective laser melting," Rapid Prototyping J.**11**(1), 26–36 (2005).
[23]Y. P Kathuria, "Microstructuring by selective laser sintering of metallic powder," Surf. Coat. Technol. **116–119**, 643–647 (1999).
[24]C. Ye, Y. Liao, and G. J. Cheng, "Warm laser shock peening driven nanostructures and their effects on fatigue performance in aluminum alloy 6160," Adv. Eng. Mater. **12**(4), 291–297 (2010).
[25]R. Fabbro, J. Fournier, P. Ballard, D. Devaux, and J. Virmont, "Physical study of laser-produced plasma in confined geometry," J. Appl. Phys. **68**(2), 775–784 (1990).
[26]K Ding and L Ye, *Laser Shock Peening: Performance and Process Simulation* (Woodhead, Cambridge, UK, 2006).
[27]Y. Liao, S. Suslov, C. Ye, and G. J. Cheng, "The mechanisms of thermal engineered laser shock peening for enhanced fatigue performance," Acta Mater. **60**(13–14), 4997–5009 (2012).
[28]P. Peyre, R. Fabbro, P. Merrien, and H. P. Lieurade, "Laser shock processing of aluminium alloys. Application to high cycle fatigue behaviour," Mater. Sci. Eng., A **210**(1–2), 102–113 (1996).

[29]E. Ganin, Y. Komem, and A. Rosen, "Shock induced hardness in α-iron," Mater. Sci. Eng. **33**(1), 1–4 (1978).
[30]D. A. Hughes and N. Hansen, "High angle boundaries formed by grain subdivision mechanisms," Acta Mater. **45**(9), 3871–3886 (1997).
[31]C. O. Mgbokwere, S. R. Nutt, and J. Duffy, "Shear band formation in 4340 steel: A TEM study," Mech. Mater. **17**(2–3), 97–110 (1994).
[32]C. S. Goh, J. Wei, L. C. Lee, and M. Gupta, "Properties and deformation behaviour of Mg–Y_2O_3 nanocomposites," Acta Mater. **55**(15), 5115–5121 (2007).
[33]M. De Cicco, H. Konishi, G. Cao, H. Choi, L.-S. Turng, J. Perepezko, S. Kou, R. Lakes, and X. Li, "Strong, ductile magnesium-zinc nanocomposites," Metall. Mater. Trans. A **40**(12), 3038–3045 (2009).
[34]Z. Zhang and D. L. Chen, "Consideration of Orowan strengthening effect in particulate-reinforced metal matrix nanocomposites: A model for predicting their yield strength," Scr. Mater. **54**(7), 1321–1326 (2006).
[35]T. W. Clyne and P. J. Withers, *An Introduction to Metal Matrix Composites*, Cambridge Solid State Science Series (Cambridge University Press, 1993), pp. 371–372.
[36]M. F. Ashby and L. Johnson, "On the generation of dislocations at misfitting particles in a ductile matrix," Philos. Mag. **20**(167), 1009–1022 (1969).
[37]R. J. Arsenault and N. Shi, "Dislocation generation due to differences between the coefficients of thermal expansion," Mater. Sci. Eng. **81**, 175–187 (1986).
[38]Y. K. Zhang, J. Z. Lu, X. D. Ren, H. B. Yao, and H. X. Yao, "Effect of laser shock processing on the mechanical properties and fatigue lives of the turbojet engine blades manufactured by LY2 aluminum alloy," Mater. Des. **30**(5), 1697–1703 (2009).
[39]D. Devaux, R. Fabbro, L. Tollier, and E. Bartnicki, "Generation of shock waves by laser-induced plasma in confined geometry," J. Appl. Phys. **74**(4), 2268–2273 (1993).
[40]K. Luo, J. Lu, L. Zhang, J. Zhong, H. Guan, and X. Qian, "The microstructural mechanism for mechanical property of LY2 aluminum alloy after laser shock processing," Mater. Des. **31**(5), 2599–2603 (2010).
[41]I. Nikitin and M. Besel, "Residual stress relaxation of deep-rolled austenitic steel," Scr. Mater. **58**(3), 239–242 (2008).
[42]B. Pinheiro, J. Lesage, I. Pasqualino, N. Benseddiq, and E. Bemporad, "X-ray diffraction study of microstructural changes during fatigue damage initiation in steel pipes," Mater. Sci. Eng., A **532**, 158–166 (2012).
[43]I. Shao, P. M. Vereecken, C. L. Chien, P. C. Searson, and R. C. Cammarata, "Synthesis and characterization of particle-reinforced Ni/Al2O3 nanocomposites," J. Mater. Res. **17**(06), 1412–1418 (2002).
[44]L. Thilly, M. Véron, O. Ludwig, and F. Lecouturier, "Deformation mechanism in high strength Cu/Nb nanocomposites," Mater. Sci. Eng., A **309–310**, 510–513 (2001).
[45]L. Thilly, M. Véron, O. Ludwig, F. Lecouturier, J. P. Peyrade, and S. Askénazy, "High-strength materials: in-situ investigations of dislocation behaviour in Cu-Nb multifilamentary nanostructured composites," Philos. Mag. A **82**(5), 925–942 (2002).
[46]A. Sanaty-Zadeh, "Comparison between current models for the strength of particulate-reinforced metal matrix nanocomposites with emphasis on consideration of Hall–Petch effect," Mater. Sci. Eng., A **531**, 112–118 (2012).
[47]Z. Zhang and D. L. Chen, "Contribution of Orowan strengthening effect in particulate-reinforced metal matrix nanocomposites," Mater. Sci. Eng., A **483–484**, 148–152 (2008).
[48]E. Nembach, *Particle Strengthening of Metals and Alloys* (John Wiley, New York, 1997).
[49]Y. Harada and K. Mori, "Effect of processing temperature on warm shot peening of spring steel," J. Mater. Process. Technol. **162–163**, 498–503 (2005).
[50]J. Y. Hwang, A. Neira, T. W. Scharf, J. Tiley, and R. Banerjee, "Laser-deposited carbon nanotube reinforced nickel matrix composites," Scr. Mater. **59**(5), 487–490 (2008).
[51]C. Ye and G. J. Cheng, Laser shock peening of nanoparticles integrated alloys: Numerical simulation and experiments," J. Manuf. Sci. Eng. **132**(6), 061017 (2010).